JTTEE5 11:75-85

Peer Reviewed

Independent Control of HVOF Particle Velocity and Temperature

T.C. Hanson, C.M. Hackett, and G.S. Settles

(Submitted 19 October 2000; in revised form 9 February 2001)

Independent control of high velocity oxygen fuel (HVOF) spray particle velocity and temperature has not been possible in the past, confusing the effect of either parameter on coating properties. This study describes a method by which velocity and temperature may be varied independently. Commercial HVOF equipment that was fitted with a special conical supersonic nozzle having four distinct particle injection locations was used. The present results, which were predicted in simulations and demonstrated in experiments, revealed several pertinent facts. First, particle velocity is principally related to combustion chamber pressure and is relatively unaffected by other design or operating conditions. Second, particle temperature is related to particle residence time within the nozzle, which can be controlled by the choice of particle injection location. In these experiments, the impact velocity and temperature of stainless steel particles were controlled within the ranges 340 to 660 m/s and 1630 to 2160 K, respectively. This range of parameters produced significant variations in splat morphology, coating microstructure, and coating oxide content. Such particle control allows the effects of velocity and temperature on coating properties to be assessed and controlled independently. These results also have commercial application, potentially enabling the user to tailor particle impact velocity and temperature to achieve specific coating properties.

Keywords deposition, high velocity, HVOF, spray

1. Introduction

In all thermal spray processes, particles are accelerated and heated by a gas as they are transported to a surface. The thermal spray community has recognized for some time that both the velocity and temperature of spray particles on impact are important parameters for determining the properties of thermally sprayed coatings. It is generally understood that particle velocity and temperature influence the coating microstructure and, thus, its physical properties.

In most studies of sprayed coating formation, an individual particle impact, or splat, is considered the building block of the sprayed coating. Thus, in characterizing the splat, one also begins to characterize the full coating. The effects of impact velocity and temperature on splat characteristics have been studied by a number of researchers.[1-9] Houben[1] addressed the influence of these parameters in a combined analytical and experimental study. Alkhimov et al.[2] and McCune et al.[3] investigated a cold gas deposition process in which only the kinetic energy of the particle was responsible for its heating on impact. This research empirically identified a critical velocity for each combination of sprayed material and substrate material. When particles impacted a substrate at or above this velocity, the coating characteristics changed noticeably. In particular, the deposition efficiency increased and the coating microstructure had characteristics that were different from those of lower velocity spraying. More recent research by Dykhuizen et al.[4] has established that high bond strengths can be attained in the cold-spray process without having hot particles or a hot substrate. Furthermore, research by Gilmore et al.[5] has shown that high-deposition efficiencies can be attained in cold spray processes if the particle velocities are sufficiently high. The effect of particle temperature, however, in determining the critical impact velocity is unclear since the independent control of particle velocity and temperature has previously precluded such a study.

On the opposite end of the temperature spectrum are high-temperature plasma sprays. Research directed by Fauchais[6] and Bianchi et al.[7] has led to an improved understanding of splat formation as well as to an appreciation for the importance of particle velocity and temperature. Therefore, based on the evidence just cited, at least a qualitative correlation between particle impact properties and the characteristics of a coating has been documented.

During thermal spraying of a coating, the interaction between the gas and particle phases is essentially determined by the gas dynamics of the spray process. The connection between the gas dynamics of the process and particle velocity and temperature, however, has not been fully explored. Therefore, the understanding required to exercise control over particle velocity and temperature is not fully available. The present study, which builds on previous work conducted by the authors on the gas dynamics of high velocity oxygen fuel (HVOF) thermal sprays,[8-10] seeks to better understand the interaction between the gas and particles. An article by Dykhuisen et al.[11] also treats the topic of thermal spray gas dynamics. This knowledge then is used to control particle velocity and temperature at impact and to assess the resulting coating microstructure.

The ability to independently control particle velocity and temperature is certainly desirable. McCune et al.[3] pointed out that thermally sensitive materials (i.e., those that degrade at elevated temperature) must not be exposed to excessive heat loads. Similarly, Voggenreiter et al.[12] suggested that improp-

T.C. Hanson, C.M. Hackett, and **G.S. Settles,** The Pennsylvania State University, University Park, PA 16802. Contact e-mail: thanson@psu.edu.

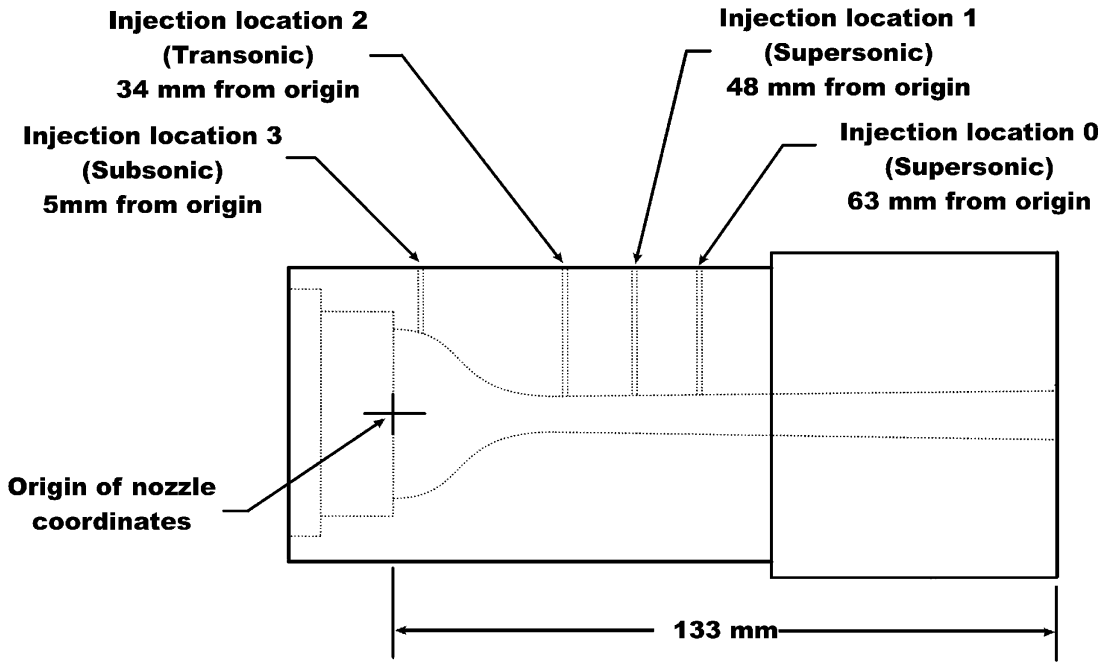

Fig. 1 Diagram of the conical nozzle indicating four injection locations

erly chosen HVOF process conditions caused sprayed metallic particles to become too hot and, thus, to degrade the coating quality. On the other hand, cold particles with low velocities may have low deposition efficiency or even an abrasive effect on the already-formed coating.

There are, then, several important reasons to have independent control of spray particle velocity and temperature. First, one can determine the separate effects of particle velocity and temperature on coating properties. This will lead to an improved understanding of bonding mechanisms, porosity formation, and other coating features. Second, one can exploit such understanding to tailor the deposition process to produce coatings with desired properties. Given the broad range of coatings available to the HVOF process, this opens many useful possibilities. Using this approach, it may be possible, for example, to create a graded coating that has one dominant characteristic, such as improved bonding, near the substrate interface, and another, such as corrosion resistance, at the surface.

In the present study, a method to independently vary particle velocity and temperature is proposed based on a fundamental understanding of the gas dynamics of the spray process. While the investigation involved both numerical modeling and experimental work, the emphasis here is on the results of the experiments. Furthermore, although the study was performed using HVOF spray equipment, the results of this research are thought to be sufficiently general that they could be applied to any thermal spray process.

2. Experimental Equipment and Methods

2.1 HVOF Spray Equipment

The spray equipment used in this study has been described in detail previously.[10] Therefore, only the features that are pertinent to the present experiments will be reviewed here. The HVOF gun, a modified Tafa JP-5000 system (Praxair-Tafa, Concord, NH), incorporates a custom converging-diverging (de Laval) nozzle with a conical supersonic section. This nozzle, which is illustrated in Fig. 1, is designed to produce Mach 2 exit flow. It has an 8 mm throat diameter, an 11 mm exit diameter, and a 133 mm effective length. The nozzle features four radial powder injection locations positioned at different axial locations along the length of the nozzle. Two injection locations, labeled 0 and 1, are located downstream of the nozzle throat in the supersonic region. Injection location 2 is effectively at the nozzle throat, while injection location 3 is located in the subsonic region, upstream of the throat. The reason for these particular locations is to provide a wide range of particle temperatures, as discussed in more detail later.

The HVOF torch burns kerosene with gaseous oxygen. It operates over a relatively wide range of chamber pressure, from 0.4 to 0.9 MPa. The particular operating conditions for these experiments were chosen to provide stoichiometric combustion chemistry, and thus nearly the same combustion temperature, for all conditions. Measurements of particle velocity and temperature were acquired over this range of chamber pressure with particles injected at each of the four injection locations.

2.2 Choice of Particles

A gas-atomized 316L stainless steel powder (1236F, Praxair-Tafa) with a mean particle size of 38 μm and a standard deviation (SD) of 11 μm was used for these experiments. Some of the results reported came from experiments performed with powder that had an average particle diameter of 44 μm. Of the many possible choices, this powder was chosen for its usefulness in corrosion protection and its sensitivity to oxidation.

2.3 Particle Velocity Measurements

The particle-trace velocimetry technique has been described previously,[10] and is reviewed here briefly. The method is similar to a time-of-flight technique,[13,14] in which the "trace" distance traveled by a luminous particle over a known time interval is measured. An intensified-charge coupled device video camera (model ISG-250, Xybion Electronic Systems Corp., San Diego, CA) with an adjustable, precisely gated, short exposure period was used with telephoto optics to record the glowing particle streaks in the field of view. A set of these images was digitized and enhanced with image processing. The streak lengths subsequently were measured, and the velocity of each particle was found simply from the length of the trace divided by the time of exposure. Statistics on the distribution of particle velocities, primarily due to the finite range of particle sizes used in the experiment, also were obtained. The uncertainty in velocity, calculated by standard methods,[15] was on the order of 12 m/s (2 to 4%) and arose principally from uncertainty in the measured lengths of the particle traces.

2.4 Particle Temperature Measurements

The two-color pyrometry technique used here to measure particle temperatures has been used by the thermal spray community in various forms for some time.[16-20] The technique is based on standard radiation thermometry practice (e.g., see Ref 20) that has been developed for the noncontact measurement of surface temperatures.

The main pyrometry system used in this study was a two-color pyrometer (model IPP-2010, Inflight, Idaho Falls, ID) that was developed specifically for measuring particle temperatures in thermal sprays. The device consisted of an optical head, a fiber-optic cable, and a unit that contained instrumentation for signal analysis and data acquisition. A cylinder, approximately 1 cm in diameter and 2 cm in length, defined the measurement volume. The calibration on the device suggested that an uncertainty band of ±5% of the temperature reading (in °C) was appropriate.

2.5 Spraying of Splats and Coatings

A gas-atomized 316L stainless steel powder (1236F, Praxair-Tafa) with a mean particle size of 38 μm and an SD of 11 μm was used for these experiments. Particle velocities and temperatures measured at a standoff distance (z) of 0.4 m from the nozzle exit, which was the position of the substrate during spraying, are reported here. To gather qualitative information about particle velocity and temperature at impact, splats were collected on glass and aluminum substrates by passing the substrate through the particle stream once at 0.25 m/s at a standoff distance of 0.4 m. Using this method, a number of splats were collected on the substrate with little or no overlapping or layering.

In addition to these splats, coatings also were deposited on aluminum and steel substrates. Typically, 10 passes through the particle stream were made in spraying these coatings. The metallographic preparation and evaluation consisted of mounting, polishing, and etching the coatings. An electrolytic etch in a 10% oxalic acid solution served to make the splat boundaries, grain boundaries, and oxidized regions of the coating visible.

2.6 Coating Porosity Measurements

The etched cross-sections under low magnification provided a means to compare the porosity of the coatings through analysis of the images. After digitizing the micrographs, areas that were considered porous were marked using image-processing software. By using a digital filter and an area measurement tool, estimates of the porous area of the cross-sections were obtained. According to the Delesse principle (e.g., see Ref 21), if the porosity is randomly distributed throughout the coating, then the percentage of porous area is identically equal to the percentage of the porous volume. While the grinding and polishing of the cross-sections may have introduced certain errors (i.e., pullouts and "smeared" splats, in particular) the technique did provide a means to make at least semiquantitative porosity comparisons among the coatings.

2.7 Oxygen Content Analysis

Several coatings were removed from the substrates and sent to the LECO Corporation (St. Joseph, MI) for oxygen content analysis. A sample of unsprayed powder also was analyzed. This analysis was performed to gain a quantitative means for comparing the extent to which oxygen was present in the coatings and to confirm the relative ranking of oxide in the coatings based on the micrographs. The reported accuracy of the measurements was ±0.5% (absolute) for the levels of oxygen found in the coatings. Nonetheless, the repeatability of duplicate measurements on the coatings was within 2% of the measured value in all instances.

3. Results

3.1 Numerical Predictions

At the outset of this investigation, numerical modeling was used to predict the general influence of gas dynamics on the spray process. This effort proved to be important for several reasons. First, it was a time-effective way to investigate parametric effects on the spray process without actual experiments. Second, even the relatively simple model employed here accurately predicted trends in HVOF gas-particle interactions. Third, it was from these predictions that the means to independently vary particle velocity and temperature was first recognized, and later demonstrated by experiments.

The prediction method used here is described in detail elsewhere,[22-25] so only a brief description is given. The gas flow within the HVOF gun was calculated using one-dimensional ideal gas dynamics. To model the effects of combustion, adiabatic flame temperature calculations yielded the gas temperature, composition, and thermodynamic and transport properties. With a full solution of the gas-flow field available, the motion of a single particle along the nozzle centerline was calculated using a Lagrangian dynamics approach, which was deemed appropriate for low-particle-density flows of this type. The particle position was determined using a Runge-Kutta integration method implemented in a FORTRAN computer code. For the purposes of this study, only the internal nozzle flow was considered, since particle acceleration and heating occur predominantly within the nozzle.

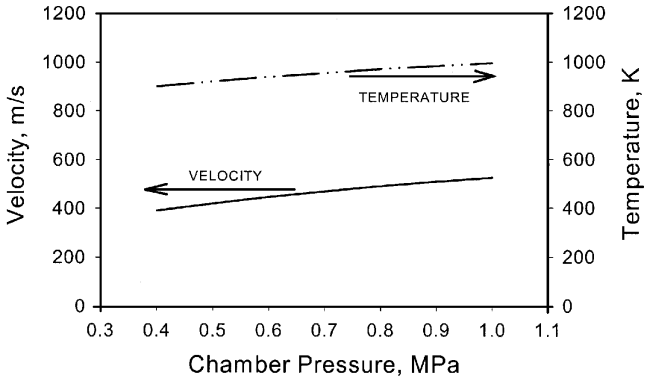

Fig. 2 Calculated velocity and temperature of a 38 μm stainless steel sphere at the exit of the conical nozzle for range of chamber pressures

There are two nozzle parameters of interest in these computations of particle velocity and temperature. The effect of chamber pressure (P_c) is shown in Fig. 2. It is evident from the plotted data that P_c has a more dramatic effect on velocity, which increases about 34% over the available range, than on temperature, which increases only 10% for a similar range of pressure. In a thermal spray nozzle, the dynamic pressure acting on the particle largely controls its acceleration. The combustion chamber pressure and dynamic pressure are directly related through the density of the gas flow. Particle temperature, however, although influenced slightly by the chamber pressure, is more strongly related to the residence time of the particle in the high-temperature gas flow. This residence time is determined by the location at which a particle is injected into the gas-flow field, which is our second parameter of interest.

The importance of injection location on particle temperature is shown in Fig. 3, where particles injected at locations 1, 2, and 3 (identified previously in Fig. 1) are predicted to exit the nozzle with different temperatures. Similarly, the calculated residence times of these three cases are also shown in Fig. 3. Residence time, and thus particle temperature, may be controlled through the choice of injection location. Furthermore, much as P_c has a weak influence on particle temperature, injection location has little effect on particle velocity.[9] With regard to particle acceleration, the injection location and dynamic pressure compensate for each other, and thus the particle velocity at the nozzle exit is nearly the same for all injection locations.

Based on the above discussion, it seems clear from the computations that one can substantially vary particle temperature with little change in particle velocity through the use of carefully selected particle injection locations. Furthermore, the use of a single injection location accompanied by changes in P_c produces a wide variation in particle velocity with only a slight effect on temperature. In this manner, independent control of particle velocity and temperature is possible. The experiments described in the ensuing sections of this article were carried out to verify this hypothesis.

3.2 Particle Measurements, Splats, and Coatings

The experimental results, which consist of velocity and temperature measurements as well as observations of splats and coating microstructures, are grouped according to the particular particle injection location used in the HVOF nozzle. Although the mechanisms by which the different types of splats and microstructures were formed are certainly of interest, the micrographic images are included principally to demonstrate that the range of particle velocity and temperature that was considered in these experiments produces noticeably different impact patterns. The scope of the present study does not allow consideration of the detailed mechanisms of splat formation or the full characterization of coating properties.

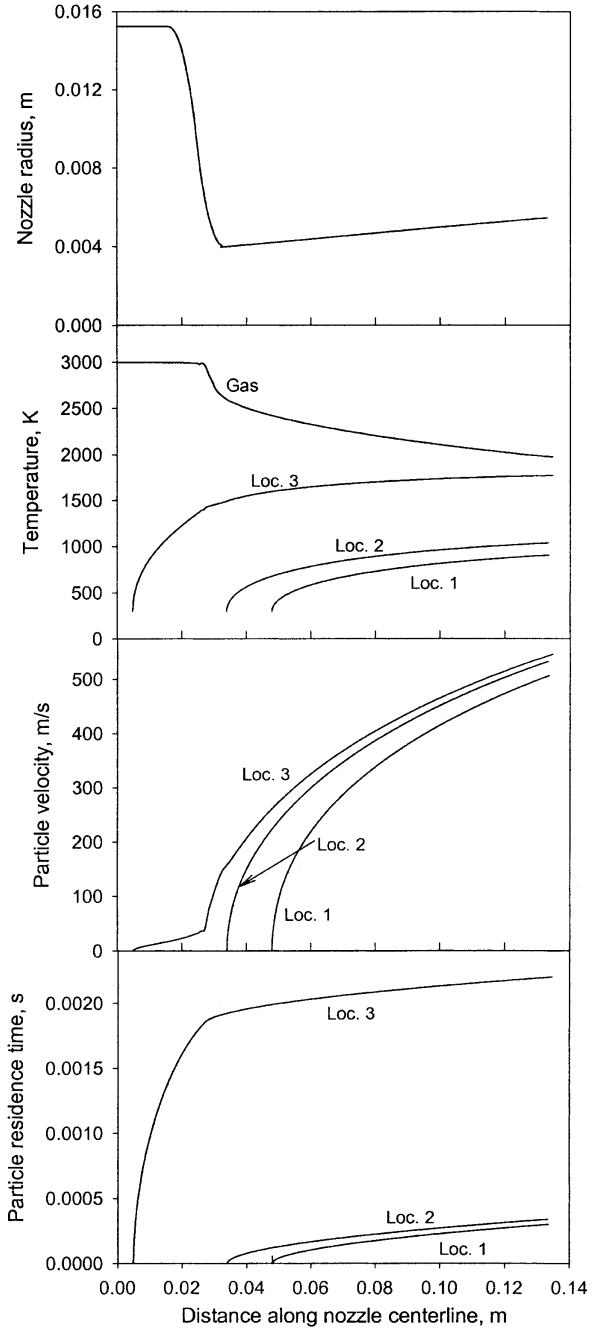

Fig. 3 Calculated temperature, velocity, and residence time of a 38 mm stainless steel sphere injected at axial locations in the conical nozzle

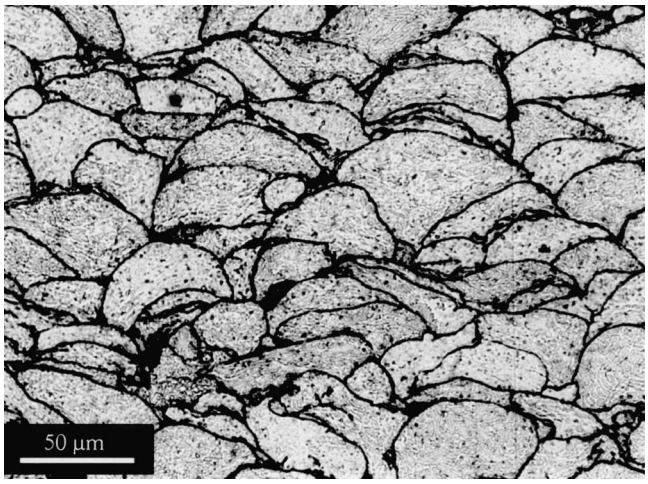

Fig. 4 Micrograph of coating sprayed with particles injected at location 0. P_c = 0.5 MPa; V_p = 380m/s; and T_p = 1550 K

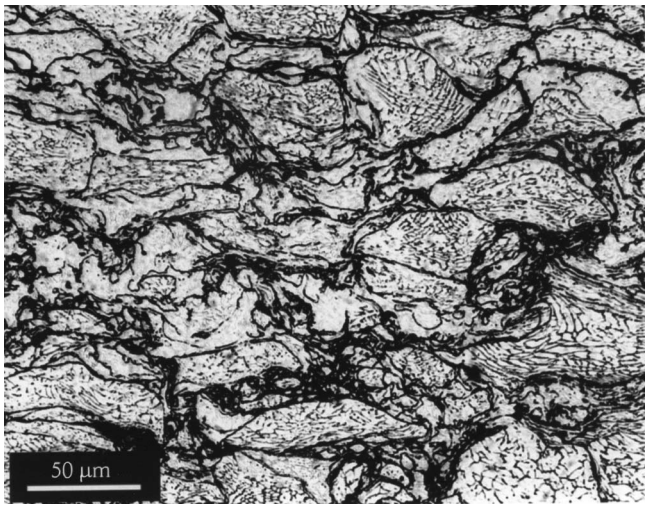

Fig. 5 Micrograph of coating sprayed with particles injected at location 0. P_c = 0.9 MPa; V_p = 660 m/s; T_p = 1740 K

Injection Location 0. This location, which was positioned downstream of the nozzle throat where the Mach number was about 1.6, proved to be the easiest at which to operate. Since the static pressure in the nozzle at this point was well within the operating pressure range of the powder feeder, there were no difficulties injecting powder into the gun. In addition, no obstruction existed between the injection point and the nozzle exit, unlike at locations 2 and 3, where the nozzle throat may have interfered with particle trajectories.

At a chamber pressure of 0.5 MPa, the particle temperature and velocity were measured as 380 ± 80 m/s and 1550 ± 60 K, respectively. The ± values placed on the velocity are based on the SD of the measurement. Since this condition was extreme in that these were both the slowest and coolest particles sprayed in the test matrix, the coating was expected to possess extreme characteristics. Observation of cross-sectional micrographs showed that the highest porosity and lowest oxidation were associated with these conditions. Additionally, the grain boundaries of the gas-atomized powder that are visible in the micrograph (Fig. 4) provided evidence—along with the pyrometric measurements—that the particles were below the melting point (nominally, 1670 K) of the 316 stainless steel powder. While the particles were evidently not molten in flight, oxygen content analysis of the coating showed that approximately 0.24% of the coating mass was oxygen, which is 10 times the content of the unsprayed powder. This oxidation, however, was confined primarily to the splat boundaries, as evidenced by the metallography.

When the combustion chamber pressure was increased to 0.7 MPa, the velocity increased to 470 ± 110 m/s, while the temperature increased to 1630 ± 70 K. These changes correspond to increases of 24% and 5%, respectively, in velocity and temperature. Still, no particles appear to have reached their melting temperature, but the porosity of the coating was substantially reduced without a noticeable change in coating oxidation. When the chamber pressure was increased further to 0.9 MPa, the mean particle velocity was 660 ± 80 m/s, and the corresponding particle temperature was 1740 ± 70 K. The optical micrograph of this coating, shown in Fig. 5, was characterized by highly deformed particles and low porosity, but also by some molten fraction and extensive oxidation. While oxidation traditionally has been considered detrimental to coating corrosion performance, recent research by Sturgeon and Buxton[26] has shown that porosity is a cause for greater concern. As a result, while the coating shown in Fig. 5 is oxidized to an extent greater than that shown in Fig. 4, it may well be better able to resist corrosion.

Injection Location 1. This location is positioned 16 mm downstream of the nozzle throat where the Mach number is approximately 1.4. Velocity measurements taken for this injection location were generally within the SD of the measurements taken at location 0 and were not consistently above or below those measurements, confirming the hypothesis that changes in injection location do not significantly affect particle velocity. Particle temperature, however, was expected to be higher at location 1 than at location 0, and this was confirmed by the pyrometric measurements. The average particle temperatures for P_c = 0.5 MPa was 1620 ± 80 K, representing about a 5% increase based on injection location. The optical micrograph of particle splats on a glass substrate in Fig. 6(a) shows that few of the particles impacting the smooth surface actually adhered. A scanning electron microscope (SEM) image of splats on a more ductile aluminum substrate (Fig. 6b) reveals some surface cratering deformation of the aluminum with adherent particles, which retain much of their spherical shape after impact. Under these conditions, coatings are still predominantly formed of softened, but not molten, particles. The cross-sectional metallograph of such a coating, pictured in Fig. 7, accordingly reveals a coating formed of splats that have retained some of their original spherical shape. The individual splats as well as the original grain boundaries within each splat are clearly visible. These grain boundaries are distorted in some areas of the coating, indicating that strain hardening has occurred during deposition. None of the splats appear to have reached their melting temperatures. Finally, there are some voids, which are visible as dark areas in Fig. 7, present along the splat boundaries.

At injection location 1, with its higher chamber pressure condition (0.7 MPa), the particle temperature was 1680 ± 80 K with

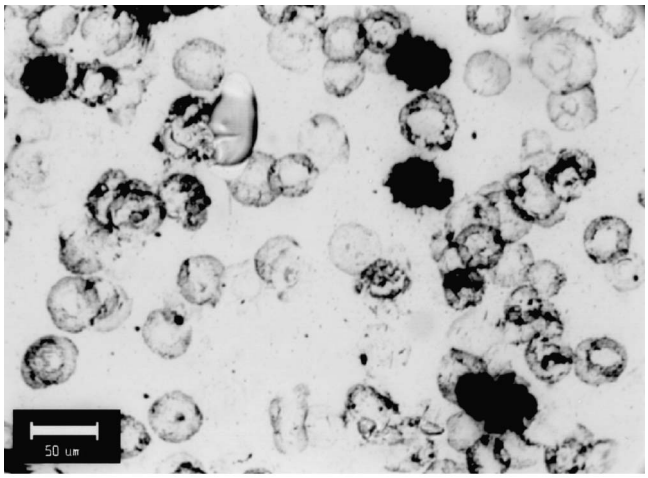

(a)

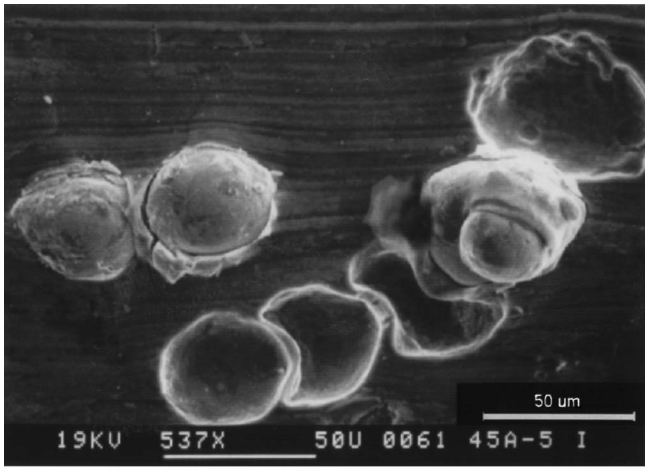

(b)

Fig. 6 Micrographs of stainless steel splats of particles injected at location 1 with P_c = 0.5 MPa. **(a)** Optical micrograph of glass substrate; and **(b)** SEM of aluminum substrate. Note that the light-colored regions visible in **(a)** are craters left by unadhered particles.

a velocity similar to that measured at location 0 at the same pressure. The corresponding optical micrograph of the glass-substrate splats (Fig. 8a) reveals larger splats and improved deposition efficiency compared to the previous case (0.5 MPa), which had about the same particle temperature but significantly lower velocity at impact. The SEM image of the aluminum substrate (Fig. 8b) reveals that some of the splats are flattened, while others retain a roughly spherical shape. Considering the proximity of the temperature measurement to the liquidus of the sprayed material (1670 K), this is consistent with the view that some particles are heated above the melting temperature, while marginally cooler particles remain solid or "doughy." It is notable that, despite the small relative increase in temperature between the 0.5 and 0.7 MPa cases, this increase occurs in a regime where the material properties change rapidly with temperature. The substrate was deformed to a greater degree and there appear to be fewer unfilled craters than in the previous case. The coating cross-section at this condition, shown in Fig. 9, indicates the

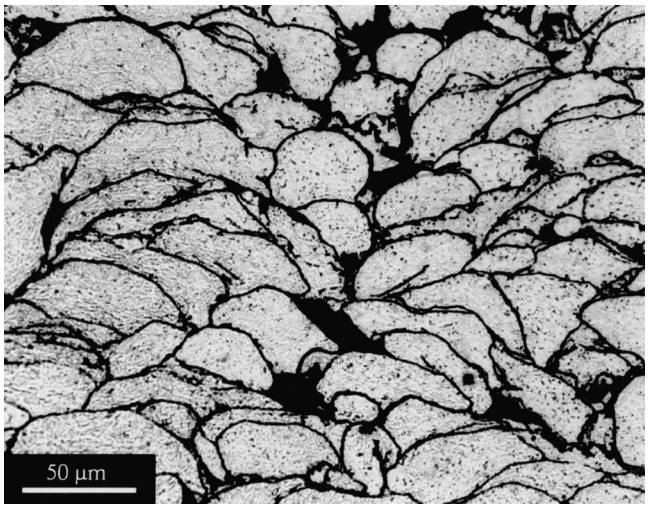

Fig. 7 Micrograph of stainless steel splats of particles injected at location 1 with P_c = 0.5 MPa, V_p = 345 m/s, and T_p = 1620 K

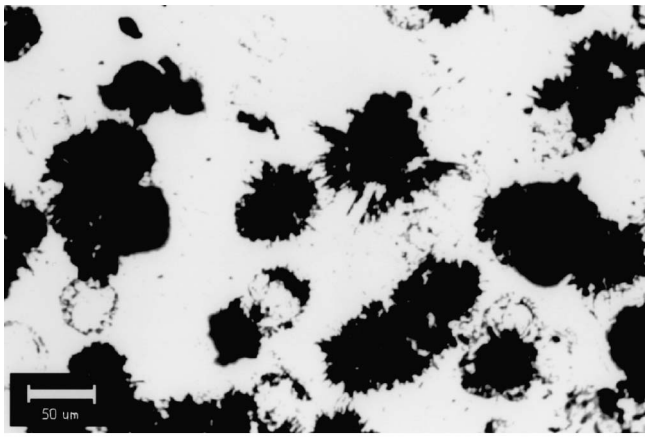

(a)

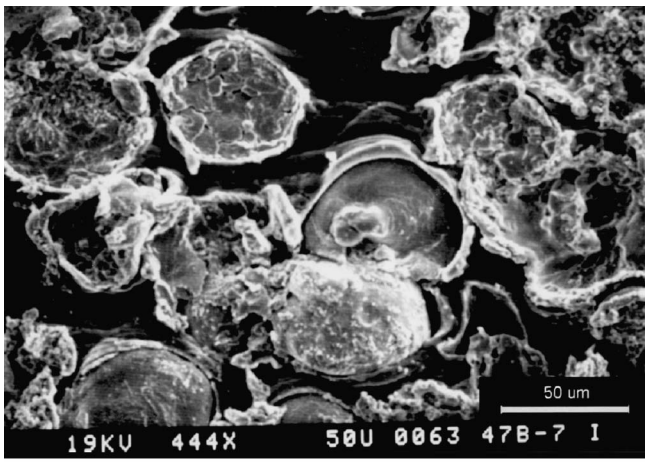

(b)

Fig. 8 Micrographs of stainless steel splats of particles injected at location 1 with P_c = 0.7 MPa. **(a)** Optical micrograph of glass substrate; and **(b)** SEM of aluminum substrate

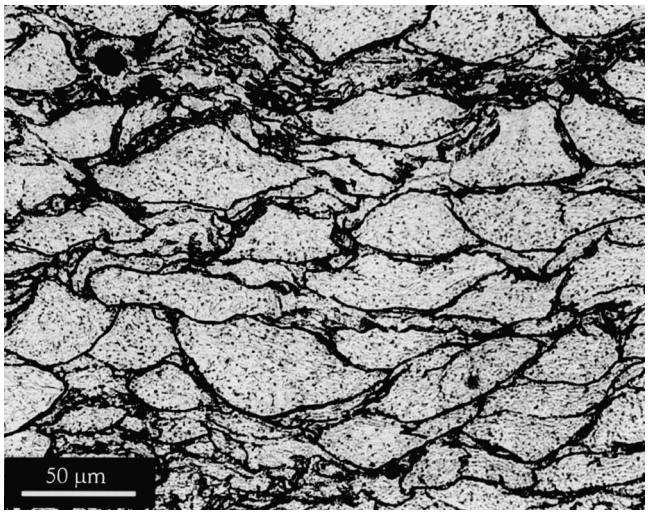

Fig. 9 Cross-sectional micrograph of an etched stainless steel coating sprayed with particles injected at location 1. P_c = 0.7 MPa; V_p = 510 m/s; and T_p = 1680 K

hibit a greater degree of deformation due to the higher impact velocity at this condition. However, a distorted fine-grain structure in many individual splats is still present, indicating that these did not melt.

Injection Location 2. At this location, particles were introduced near the nozzle throat where the freestream Mach number was 1.1. Velocity measurements were not made with particles injected at this location, since little difference was expected based on injection location. Particle temperatures, however, were expected to be higher due to the increased residence time of particles injected at location 2 compared to location 1. For example, at P_c = 0.5 MPa, the measured particle temperature was 1900 ± 300 K, which is about 280 K higher than for particles injected at location 1. The temperature measurements of the powder injected at locations 2 and 3 were preliminary, having been performed by an experimental pyrometer with a limited calibration and a considerably larger error bar than that of the instrument manufactured by Inflight that was described previously.

The corresponding optical micrograph of splats on a glass substrate (Fig. 10a) shows even more adhered particles than in the previous cases. There is, however, still some evidence of particle rebound resulting in unfilled craters in the substrate. Furthermore, the presence of radially ejected material around the edge of some splats indicates that these particles were at least semimolten on impact. The SEM image of the aluminum substrate (Fig. 10b) reveals a flat, fractured splat surface, further indicating the impact of semimolten particles.

Figure 11, the corresponding metallographic cross-section, shows some flattened splats interspersed with less-defined regions within the coating. Those original splats that remain distinct within this coating also have their original grain boundaries preserved, although in a highly deformed state. The other regions appear to be material that has melted, resolidified, and partially oxidized in the coating. The combination of these microstructural characteristics indicates that the physical properties of the coating may vary substantially throughout its thickness.

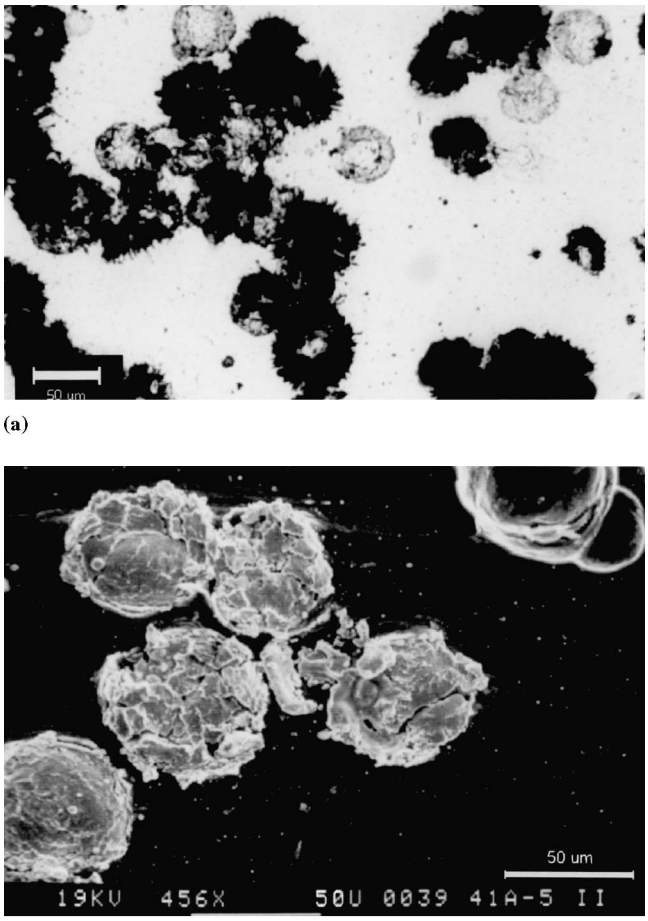

(a)

(b)

Fig. 10 Micrographs of stainless steel splats of particles injected at location 2 with P_c = 0.5 MPa. **(a)** Optical micrograph of glass substrate; and **(b)** SEM of aluminum substrate

These observations demonstrate that a change of 280 K in particle temperature, particularly if particle melting occurs in this range, can greatly change splat morphology within the coating.

Injection Location 3. This location is positioned 28 mm upstream of the nozzle throat where the Mach number is less than 0.3. Particle injection there proved to be challenging due to the limitations on the powder feeder operating pressure that were mentioned previously. Measurements at chamber pressures of 0.4 and 0.5 MPa confirmed that the injection location had little effect on particle velocity; these results corresponded well with those of particles injected at location 1. At P_c = 0.5 MPa, the particle velocity and temperature were measured to be 370 ± 90 m/s and 2160 ± 370 K, respectively. This temperature was 250 K, or 14%, higher than that for location 2 and was 540 K, or 33%, higher than that for location 1, as was expected based on the computations described earlier.

The splat patterns for injection location 3 reveal several interesting features that were not encountered previously in this study. As seen in Fig. 12(a), the splats are considerably smaller than those observed previously and are very irregular in shape. There also appear to be small deposits of ejected material scattered between the main splats on the substrate surface. The SEM

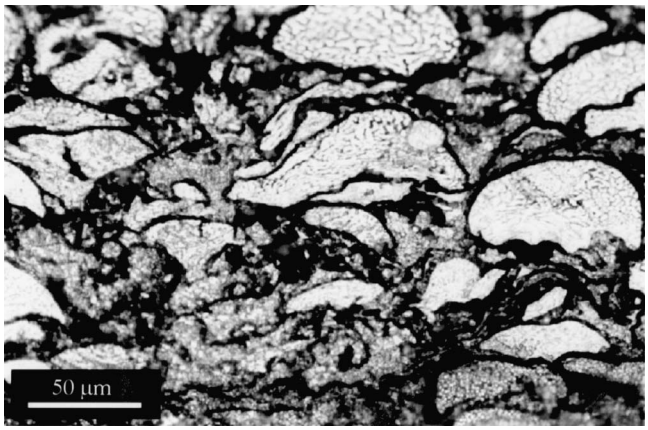

Fig. 11 Cross-sectional micrograph of an etched stainless steel coating sprayed with particles injected at location 2 with P_c = 0.5 MPa. T_p = 1900 K

images (Fig. 12b and c) show that there is little, if any, deformation of the aluminum substrate. Most of the particle mass appears to have splashed away from the center of the splat. The highly magnified SEM image (Fig. 12c) shows a splat approximately 20 μm in diameter with many of the characteristics that one would expect from the impact of a liquid droplet, as first demonstrated by Edgerton.[27] The deposition efficiency of liquid droplet impact is expected to be less than that for solid or semisolid impact, due to splatter and splash-back phenomena.

No cross-sectional micrographs that were suitable for presentation were obtained from coatings as a result of particles injected at location 3. However, it can be said that these coatings appear to show few intact splat boundaries and no visible fine-grain structure, very likely due to the particles being fully molten on impact.

3.3 Discussion of Particle Velocity and Temperature Measurements

The influence of chamber pressure on measured particle velocity is shown in Fig. 13. Nearly a twofold increase in particle velocity (340 to 660 m/s) measured 0.4 m from the nozzle exit is evident over the range of chamber pressures tested here. Thus, as predicted earlier in Fig. 2, chamber pressure is a viable means to control the velocity of particles at impact.

The dependence of particle temperature on injection location is shown clearly in Fig. 14, where measured temperatures are plotted against chamber pressure for injection locations 1 and 2. The 14 mm change in injection location had an effect on temperature that is of similar magnitude to the effect of doubling the combustion pressure. For each pressure condition, a measurable difference in temperature is apparent for particles injected at each location, which also is as expected. Thus, it is clear that the initial hypothesis of this investigation, that independent control of particle velocity and temperature can be achieved through the choice of chamber pressure and injection location, is confirmed by these experimental results. It must be noted that changing combustion pressure or injection location alone does not afford independence; independent control is made possible with appropriate changes in both variables. The range of particle velocity

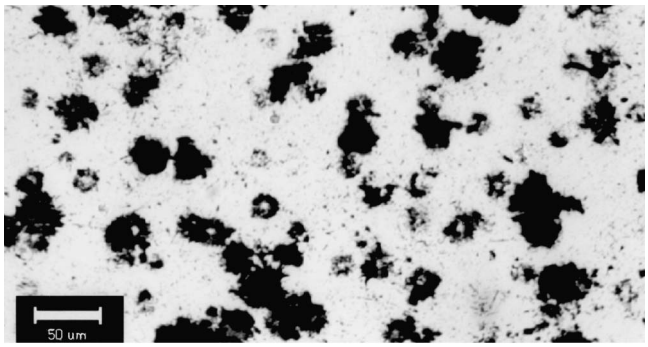

(a)

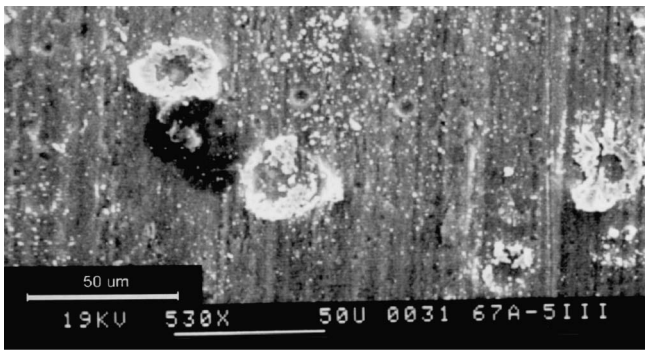

(b)

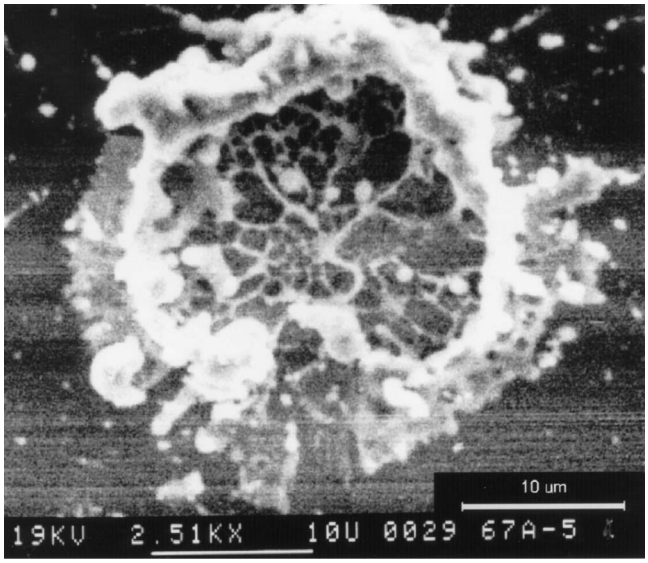

(c)

Fig. 12 Micrographs of stainless steel splats of particles injected at location 3 with P_c = 0.5 MPa. **(a)** Optical micrograph of glass substrate; **(b)** SEM of aluminum substrate; and **(c)** high-magnification SEM image

and temperature that is accessible through this means produces a wide range of splat and coating characteristics of sprayed stainless steel. One can assume that a similar range of coating properties is produced as well. However, the correlation of coating properties with particle velocity and temperature for various types of coatings is a topic for future study.

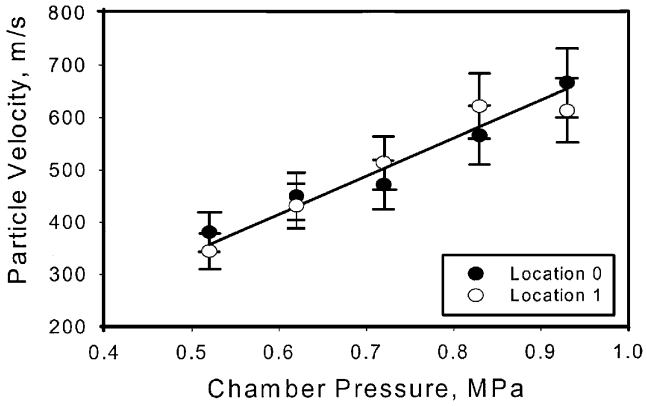

Fig. 13 Measured velocity of 38 μm mean diameter stainless steel particles at z = 0.4 m standoff distance for a range of chamber pressure conditions and two injection locations. Bars on the data points indicate the SD of the measurements.

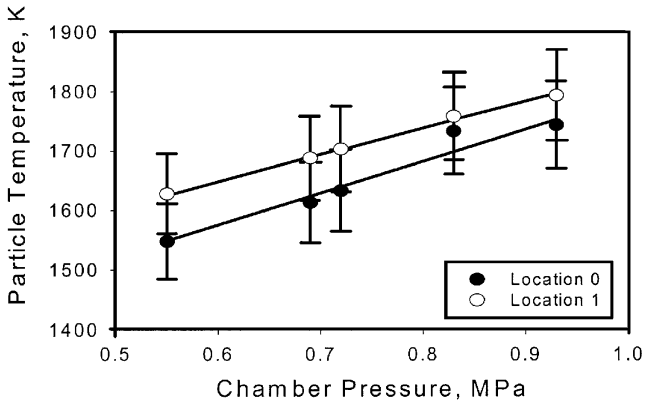

Fig. 14 Influence of the injection location on measured particle temperature at a standoff distance of 0.4 m for a range of chamber pressure conditions

3.4 Discussion of Coating Oxidation Measurements

Quantitative data from a chemical analysis of the sprayed coatings provided a means to observe the effect of particle temperature on coating oxidation. From an analysis of the images, it was expected that quantitative analysis of the coatings that were formed of hot particles would have a higher oxygen content than the coatings that were formed from cooler particles. This expectation was generally observed, as shown in Fig. 15, despite the small number of samples that were analyzed. In particular, as average particle temperatures rose above the liquidus of the metal (1670 K), the oxygen content in the samples began to increase dramatically.

3.5 Discussion of Coating Porosity Measurements

The relation of coating porosity to chamber pressure is shown for injection locations 1 and 2 in Fig. 16. A few trends are evident. At the lower chamber pressures, in which the particles

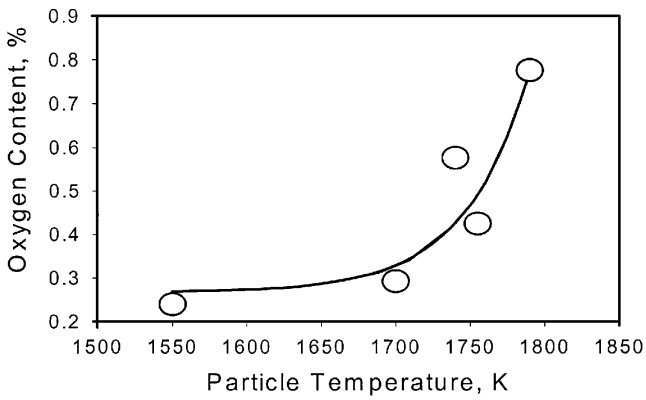

Fig. 15 Relation of particle temperature on mass oxygen content in HVOF sprayed coatings

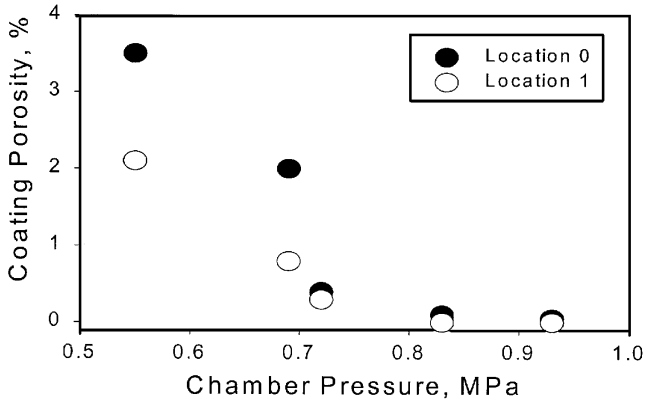

Fig. 16 Effect of injection location and chamber pressure on coating porosity

were below their melting temperature, the hotter particles (i.e., the particles injected at location 1) created denser coatings than their cooler counterparts. As shown earlier, injection location has little effect on particle velocity, so the differences in porosity at a given chamber pressure illustrate the effect of temperature alone. Since the higher chamber pressures correspond with significant fractions of fully molten particles, the near-zero porosity of these coatings is likely to be neither an effect of particle temperature alone nor an effect of particle velocity alone. A more thorough understanding of the separate effects of particle velocity and temperature will be possible with experiments that keep the particle temperatures below the melting point. Nonetheless, if one is willing to accept the inherently high levels of oxidation, molten spray particles can provide coatings with minute porous volume fractions.

4. Conclusions

In this study, the means for independent control of particle velocity and temperature has been demonstrated through the use

of an HVOF thermal spray torch that has a conical supersonic nozzle with several different particle injection locations. The means for such control was anticipated from numerical modeling of the influence of gas dynamics on particle acceleration and heating, which indicated that chamber pressure could be used to control particle velocity without a strong influence on temperature. Conversely, particle injection location was found to determine the residence time of particles within the nozzle, thus providing a means to control particle temperature. Finally, injection location had a negligible effect on particle velocity according to the numerical model.

A set of experiments was devised to determine whether such independent particle velocity and temperature control could be achieved in practice. The results of these experiments were positive, revealing that the impact velocity and temperature of 38 μm stainless steel particles could be controlled within the ranges 340 to 660 m/s and 1630 and 2160 K, respectively. Most importantly, it was demonstrated that a range of temperature variation was available without a significant velocity variation. Similar findings were demonstrated for the control of velocity independently of temperature. Finally, a significant range of stainless steel splat and coating microstructure characteristics was found for such variations in particle parameters prior to impact.

Although not explicitly defined here, a range of particle velocities and temperatures clearly exists within which process efficiency and coating characteristics may be optimized for a given material. In future experiments, the particle velocity and temperature will be "tailored" through variations in chamber pressure and injection location to produce desired characteristics in a particular coating system. Future research will focus on lowering particle temperatures while maintaining high particle velocities. It is anticipated that these conditions will decrease coating oxidation and porosity while promoting high deposition efficiency.

The results of this study are important for several reasons. First, a fundamental understanding of the importance of gas dynamics on particle velocity and temperature yields an opportunity to exercise greater control on these particle parameters, and, therefore, on the resulting coating properties. Second, through such an approach, an improved understanding of the mechanisms of coating formation can be attained. Third, by using independent particle velocity and temperature control, it appears possible to optimize deposition processes and coating characteristics for a given material and substrate. Finally, these results are not confined to the HVOF process and may be generalized to all thermal sprays to achieve improved process control.

Acknowledgments

The authors thank J.D. Miller of the Gas Dynamics Laboratory for his assistance in these investigations. Drs. J.W. Naughton and S.S. Garg were instrumental in the development and verification of the particle dynamics code used for modeling gas-particle interactions in HVOF flowfield. Financial support for this research was provided by U.S. Department of Energy grant DE-FG02-92ER14302, amendment A008, which was monitored by Dr. Robert E. Price.

References

1. J.M. Houben: "Future Developments in Thermal Spraying," in *2nd National Thermal Spray Conference*, ASM International, Materials Park, OH, 1984, pp. 1-19.
2. A.P. Alkhimov, V.F. Kosarev, and A.N. Papyrin: "A Method of 'Cold' Gas-Dynamic Deposition," *Sov. Phys. Dokl.*, 1990, *35*(12), pp. 1047-49.
3. R.C. McCune, J.N. Hall, A.N. Papyrin, W.L. Riggs, and P.H. Zajchowski: "An Exploration of the Cold Gas-Dynamic Spray Method for Several Material Systems," in *Advances in Thermal Spray Science and Technology*, C.C. Berndt and S. Sampath, ed., ASM International, Materials Park, OH, 1995, pp. 1-5.
4. R.C. Dykhuizen, M.F. Smith, D.L. Gilmore, R.A. Neiser, et al.: "Impact of High Velocity Cold-Spray Particles," *J. Thermal Spray Technol.*, 1999, *8*(4), pp. 559-64.
5. D.L. Gilmore, R.C. Dykhuizen, R.A. Neiser, T.J. Roemer, et al.: "Particle Velocity and Deposition Efficiency in the Cold Spray Process," *J. Thermal Spray Technol.*, 1999, *8*(4), pp. 576-82.
6. P. Fauchais: "Formation of Plasma Sprayed Coatings," *J. Thermal Spray Technol.*, 1995, *4*(1), pp. 3-6.
7. L. Bianchi, F. Blein, P. Lucchese, M. Vardelle, et al.: "Effect of Particle Velocity and Substrate Temperature on Alumina and Zirconia Splat Formation," in *Thermal Spray Industrial Applications,* C.C. Berndt and S. Sampath, ed., ASM International, Materials Park, OH, 1994, pp. 569-74.
8. C.M. Hackett, G.S. Settles, and J.D. Miller: "On The Gas Dynamics of HVOF Thermal Sprays," *J. Thermal Spray Technol.*, 1994, *3*(3), pp. 299-304.
9. C.M. Hackett and G.S. Settles: "The Influence of Nozzle Design on HVOF Spray Particle Velocity and Temperature," in *Advances in Thermal Spray Science and Technology*, C.C. Berndt and S. Sampath, ed., ASM International, Materials Park, OH, 1995.
10. C.M. Hackett: "The Gas Dynamics of High-Velocity Oxy-Fuel Thermal Sprays," Ph.D. Thesis, Penn State University, 1996. UMI order number 9628094.
11. R.C. Dykhuizen and M.F. Smith: "Gas Dynamic Principles of Cold Spray," *J. Thermal Spray Technol.*, 1998, *7*(2), pp. 205-12.
12. H. Voggenreiter, H. Huber, S. Beyer, and H.-J. Spies: "Influence of Particle Velocity and Molten Phase on the Chemical and Mechanical Properties of HVOF-Sprayed Structural Coatings of Alloy 316L," in *Advances in Thermal Spray Science and Technology*, C.C. Berndt and S. Sampath, ed., ASM International, Materials Park, OH, 1995, pp. 303-08.
13. R.J. Adrian: "Particle-Imaging Techniques for Experimental Fluid Mechanics," *Annu. Rev. Fluid Mech.*, 1991, *23*, pp. 261-304.
14. M. Gharib and C. Willert: "Particle Tracing: Revisited," *Lecture Notes in Engineering, Advances in Fluid Mechanics Measurements*, M. Gad-el-Hak, ed., Berlin, Springer, 1989, *45*, pp. 109-26.
15. H.W. Coleman and W.G. Steele: *Experimentation and Uncertainty Analysis for Engineers*, John Wiley-Interscience, New York, 1989.
16. J.R. Fincke, C.L. Jeffrey, and S.B. Englert: "In-Flight Measurement of Particle Size and Temperature," *J. Phys. E: Sci. Instrum*., 1988, *21*, pp. 367-70.
17. J.R. Fincke, W.D. Swank, and C.L. Jeffrey: "Simultaneous Measurement of Particle Size, Velocity, and Temperature in Thermal Plasmas," *IEEE Trans. Plasma Sci.*, 1990, *18*(6), pp. 948-57.
18. J. Mishin, M. Vardelle, J. Lesinski, and P. Fauchais: "Two-Colour Pyrometer for the Statistical Measurement of the Surface Temperature of Particles Under Thermal Plasma Conditions," *J. Phys. E: Sci. Instrum.,* 1987, *20*, pp. 630-35.
19. S. Kuroda: "Fundamental Phenomena in Spray Deposition of Surface Coatings," in *NRIM Research Activities*, National Research Institute for Metals Japan, Tokyo, 1992, pp. 9-10.
20. D.P. DeWitt, and G.D. Nutter: *Theory and Practice of Radiation Thermometry*, John Wiley-Interscience, New York, 1988.
21. E.E. Underwood: *Quantitative Stereology*, Addison Wesley, Reading, MA, 1970.
22. G.S. Settles, and S. Garg: "A Scientific View of the Productivity of Abrasive Blasting Nozzles," *Proc. Steel Structures Painting Council 1994 Int. Conf.*, 12-19, 1994.
23. S.S. Garg, C.M. Hackett, J.W. Naughton, and L.N. Cattafesta: "A Comparison of Drag Laws for Predicting Particle Trajectory in High-Speed

Flows," *1996 ASME Fluids Engineering Summer Meeting*, San Diego, CA, July 7-11, 1996.
24. J.W. Naughton: "The Enhancement of Compressible Turbulent Mixing Via Streamwise Vorticity," Ph.D. Thesis, Penn State University, 1993.
25. P.A. Kessel: "A Study of the Aerodynamic Design of Viscous Nozzles Used to Accelerate Large Particles to High Velocity," Ph.D. Thesis, University of Tennessee, 1977. UMI order number 7716589.
26. A.J. Sturgeon and D.C. Buxton: "The Electrochemical Corrosion Behavior of HVOF Sprayed Coatings," in *Thermal Spray Surface Engineering via Applied Research*, C.C. Berndt, ed., ASM International, Materials Park, OH, 2000, pp. 1011-15.
27. E. Jussim and G. Kayafas: *Stopping Time: The Photographs of Harold Edgerton*, H.N. Abrams, Inc., New York, 1987.